Analysis of Surface Pressure Distributions on Two Elliptic Missile Bodies

Jerry M. Allen* and James L. Pittman†
NASA Langley Research Center, Hampton, Virginia

The state-of-the-art methods for predicting missile aerodynamic characteristics do not accurately predict the loads on missile configurations with bodies of elliptic cross section. An investigation of this problem found significant nonlinear flow disturbance on the windward surface of a 3:1 elliptic body at Mach 2.50 in addition to the nonlinear vortical flows which develop on the leeside. A nonlinear full-potential flow method (NCOREL) was found to provide extremely accurate pressure estimates for attached-flow conditions and the vortex prediction method contained in a state-of-the-art method (NOSEVTX) was shown to calculate body vortices and leeside pressures.

Nomenclature

C_N = normal-force coefficient, normal force/$q_\infty S$
C_p = pressure coefficient, $p-p_\infty/q_\infty$
L = body length
M = freestream Mach number
p = local body surface pressure
p_∞ = freestream static pressure
q_∞ = freestream dynamic pressure
S = reference area
X = axial coordinate from body nose
α = angle of attack
θ = polar coordinate angle
ϕ = roll angle

Introduction

RECENT experimental research in advanced missile concepts has shown that missiles with elliptical bodies have definite aerodynamic performance and stability advantages over the conventional circular body shape.[1,2] The application of state-of-the-art missile aerodynamic prediction codes[3-5] to elliptic body missile configurations has shown relatively poor force estimates on the missile body, which is in contrast to previous results on circular-body configurations.[6-8] As a result of these findings, an experimental program was initiated to obtain detailed surface pressure and flow-visualization data on two elliptical body missile configurations. The configuration geometries were chosen to represent two models studied previously in an extensive parametric stability and control investigation of elliptic missile shape effects.[9] A large set of body pressure data was obtained for body-alone, body-tail, and body-wing-tail combinations for both bodies at a Mach number of 2.50, an angle-of-attack range of -5 to 25 deg, and roll angles from 0 to 90 deg. These data have been published recently in tabular form in a NASA document.[10]

The purpose of this paper is to investigate the reason for the relatively poor force estimates on elliptical bodies provided by state-of-the-art missile aerodynamic prediction codes and to indicate probable solutions to the problem. This analysis will be performed by extensive comparisons of experimental and calculated pressure distributions on the elliptical missile body. Also, vapor-screen photographs will be used to analyze the leeside vortex characteristics. The primary method used in the present study for predicting the aerodynamics of missile bodies at high angles of attack is the NOSEVTX code,[4] which is based on supersonic linear theory with a technique for calculating and tracking leeside vortices. A recently developed nonlinear potential flow method, NCOREL,[11] is also included in this analysis because of its capability to calculate nonlinear attached-flow characteristics.

Experimental Results

The force and moment test of Ref. 9 contained a total of nine missile configurations with bodies of elliptic cross section. The basic body longitudinal area distribution of these configurations was that of the Adams minimum drag body.[12] Two bodies of this set were chosen for more detailed analysis through pressure models and are illustrated in Fig. 1, which shows the axial stations where pressure orifices were located. At each station, the orifices were located around the entire circumference.

As can be seen in Fig. 1, the body of one configuration has a pointed nose and a 3:1 elliptical cross section along the entire length of the body. The second body has a blunt nose which blends into a 3:1 elliptical midbody which blends into a circular base. The nose bluntness on this model represents a departure from the Adams area distribution. A more complete description of these models can be found in Ref. 10. For convenience, the first model is identified in this paper as the "sharp-nosed body," and the second as the "blunt-nosed body."

The pressure and flow-visualization investigation was conducted in the low Mach number test section of the NASA Langley Unitary Plan Wind Tunnel.[13] The test was conducted at a freestream Mach number of 2.50 and a freestream Reynolds number of 2×10^6/ft.

Figure 2 shows some typical pressure distributions around the body at several angles of attack. These data were taken on the sharp-nosed body at zero roll angle at the 60% body station. This figure emphasizes the very detailed pressure data which were obtained and shows a smooth, systematic variation with angle of attack. The large pressure gradients around the leading edge are apparent, as well as the changing nature of the leeside flow with variations in angle of attack. Specifically a rather rapid leeside recompression occurs at $\alpha=5$ and 10 deg, but at $\alpha\geq15$ deg the leeside recompression

Presented as Paper 83-1841 at the AIAA Applied Dynamics Conference, Danvers, Mass., July 13-15, 1983; received July 29, 1983; revision received Dec. 28, 1983. This paper is declared a work of the U.S. Government and therefore is in the public domain.

*Aero-Space Technologist, Fundamental Aerodynamics Branch, High-Speed Aerodynamics Division. Associate Fellow AIAA.

†Aero-Space Technologist, Fundamental Aerodynamics Branch, High-Speed Aerodynamics Division. Member AIAA.

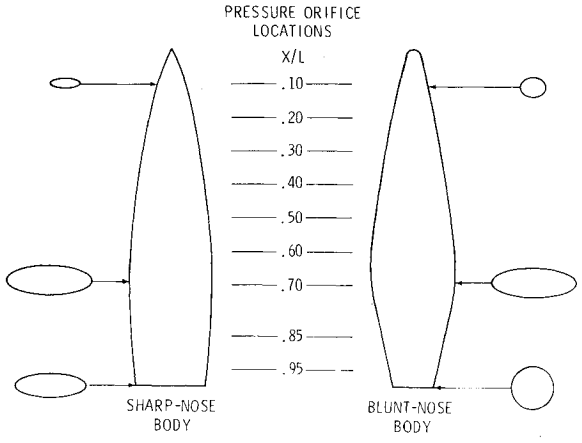

Fig. 1 Model details.

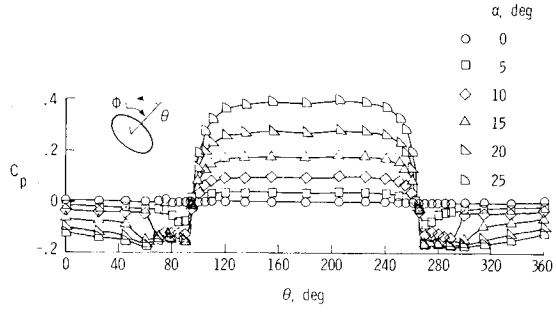

Fig. 2 Sharp-nosed body pressure distributions. $\phi = 0$ deg, $X/L = 0.60$, $M = 2.50$.

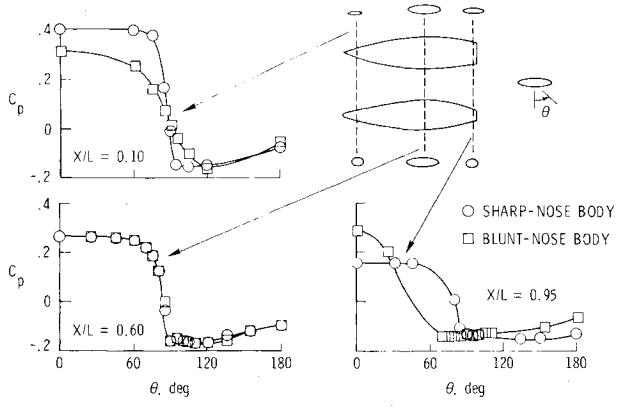

Fig. 3 Effect of body shape on pressure distributions. $\alpha = 20$ deg, $\phi = 0$ deg, $M = 2.50$.

diminishes in strength and the leeside pressures approach a plateau level, which is generally indicative of separated flow. Since the roll angle for these data was zero, pitch plane symmetry should exist. The figure shows that there is very good symmetry in the data, which gives confidence in the accuracy of the measurements.

The effects of body shape on the pressure distributions can be seen in Fig. 3, which presents the data for an angle of attack of 20 deg and zero roll angle. The cross-sectional shape of the blunt-nosed body near the nose and aft end of the body is almost circular compared to the 3:1 elliptical shape of the sharp-nosed body. Near the body midsections, however, the shape of the two bodies is very similar. The pressure distributions on these two bodies near the nose and aft ends are very different, whereas they are almost identical near the midbody sections. This result indicates that the local pressure distributions are a strong function of the local cross-sectional shape.

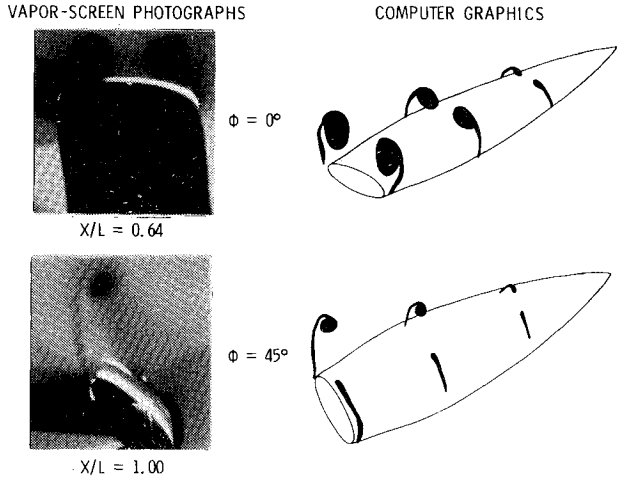

Fig. 4a Experimental vortex patterns for the sharp-nosed body. $\alpha = 20$ deg, $M = 2.50$.

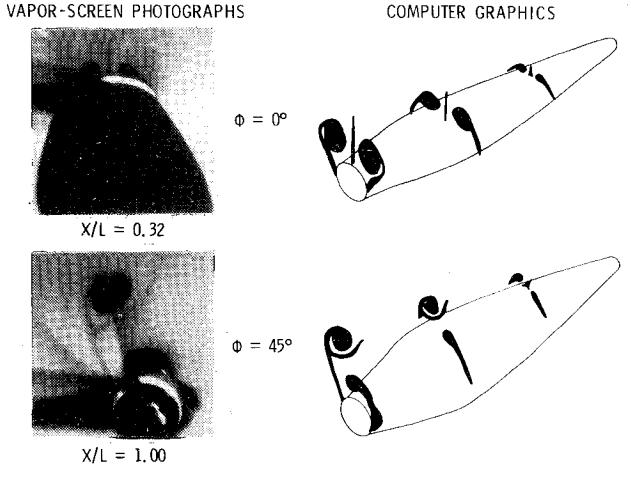

Fig. 4b Experimental vortex patterns for the blunt-nosed body. $\alpha = 20$ deg, $M = 2.50$.

Vapor-screen photographs were taken on these two configurations at several longitudinal stations to provide a better understanding of the experimental pressure data and to explore the vortex characteristics of these models. Some examples are shown in Fig. 4. To obtain a better visualization of the vortex development, the vortices were digitized from these photographs and plotted along with the numerical models of the bodies. These digitized plots are also shown in Fig. 4 for both bodies at an angle of attack of 20 deg and roll angles of 0 and 45 deg.

For the sharp-nosed body (Fig. 4a) at zero roll angle, two symmetric vortices develop near the nose of the model and continue to grow along the sides of the body. According to the pressure data presented in Fig. 2, these vortices strongly influence the leeside pressure distributions. At 45 deg roll angle the lower vortex is highly elongated and stays close to the body surface, whereas the upper vortex retains the approximate shape of the $\phi = 0$ deg vortex although it is much smaller and is located further above the body surface.

The blunt-nosed body results (Fig. 4b) at zero roll angle show that the vortices are similar to those on the sharp-nosed model. In addition to two symmetrical vortices, however, a thin vertical region develops along the top centerline of the body. This region has been observed only on blunt-nosed bodies[1] and is probably caused by flow expansion over the hemispherical nose. The region becomes highly elongated near the aft end of the body. Note from the data in Fig. 3 that at $X/L = 0.60$ this region has no measurable effect on the leeside centerline pressures.

A very unusual phenomenon is observed when this blunt-nosed body is rolled to 45 deg. The region that forms over the nose has now moved toward the top of the model and thus toward the upper vortex. At some point between the first and second vapor-screen stations, this region leaves the body and becomes attached to the feeding sheet of the upper vortex and continues to be pulled toward the vortex core.

Discussion of Computational Methods

The body component of the overall loads for a conventional circular-body missile can be relatively small, whereas for an elliptical-body missile the body contribution can be very large, as illustrated in Fig. 5. Any computational method applied to elliptical-body missiles, therefore, must be able to predict the aerodynamics of the body as well as the fins accurately. Experimental data from the sharp-nosed body will be used in this paper to evaluate two computational methods for their ability to predict the pressure distributions on such bodies.

The state-of-the-art for missile aerodynamic prediction techniques is represented by the DEMON series of codes.[3,4,14] These codes calculate the supersonic aerodynamic characteristics of complete missile configurations with circular or noncircular body cross sections. The body solutions are calculated by the NOSEVTX code[4] which utilizes the principle of superposition to combine a near-field linear-theory solution with a vortex solution. The continuous shedding of leeside vorticity is approximated by discrete vortices shed at specified intervals along the body. The superposition technique allows both the linear-theory solution and the vortex solution to be assessed independently. Previous experience with the DEMON codes has shown that they provide good estimates of overall forces and moments on conventional circular-body missiles.[6,8]

Another approach to this problem is included in the second method evaluated in this paper, the NCOREL code.[11] NCOREL is a three-dimensional finite difference code which uses an implicit marching technique to solve the nonconservative supesonic full-potential equation; it has been shown[15] to give good results for the pressure distributions on wings and aircraft fuselage-type bodies at angles of attack up to about 10 deg in supersonic flow. It has also been shown[16] to give fairly good overall normal-force and pitching-moment loads on an axisymmetric body at angles of attack up to about 20 deg at $M=2.5$ and on the sharp-nosed body of this paper up to about $\alpha=12$ deg at $M=2.0$.

The relationship between the freestream Mach cone at the body apex and the geometry of the body is an important parameter in supersonic flow. For the particular case of the sharp-nosed body at $M=2.5$, the nose of this body falls outside the freestream Mach cone, which is the supersonic leading-edge condition. Under this circumstance, the linear-theory surface-source-panel technique in the NOSEVTX code does not provide a solution. In order to obtain NOSEVTX solutions, the nose of the body was modified so that it fell within the Mach cone. This procedure tends to reduce the solution accuracy near the nose of the body; however, the effect on the body pressure downstream of the nose is probably very small.

The supersonic leading-edge condition also affects the NCOREL code in that two of the input parameters which govern the starting solution must be modified. The values of these two parameters fall within certain known bounds and are determined by the user through a trial and error procedure which can be accomplished quickly on an interactive terminal. A thorough discussion of this procedure is contained in Ref. 11.

Typical run times for the NOSEVTX and NCOREL codes were generally in the range of 5 to 10 min of CPU time on a CYBER 175 computer, although no attempt to optimize run times was made. The run times for NOSEVTX varied from about 60-170% of those of NCOREL, but neither method was consistently faster than the other. The NCOREL run times increased with angle of attack, whereas those of NOSEVTX decreased somewhat with angle of attack. At low angles of attack where no vortices developed, NOSEVTX was much faster than NCOREL. The increased run times for NCOREL at high angles of attack are due to large leeside disturbances which are calculated in the potential flow at these angles of attack.

For zero roll angle both codes were able to take advantage of flow symmetry to provide calculations only on the half-body. For the pressure calculations presented in this paper, NOSEVTX utilized 261 surface singularities and NCOREL utilized 900 grid points on the half-body surface.

Comparison and Analysis of Computational Methods and Experiment

NOSEVTX Code

Comparisons between the vortex patterns computed by NOSEVTX and vapor-screen vortices shown previously are presented in Fig. 6. In this plot, both data and theory are for the sharp-nosed body alone at $X/L=1.0$, 20 deg angle of attack, and roll angles of 0 and 45 deg. The dots are the locations of the discrete vortices at this station computed by NOSEVTX and the arrows represent their direction of rotation. The computed vortices on either side of the body have been connected in this plot to show the roll-up pattern.

At zero roll angle, the computed vortices are seen to give a very good representation of the experimental vortices. At the 45 deg roll angle, the computed roll-up pattern is not as smooth, and the agreement with the data is not as good as it was at $\phi=0$ deg; however, the essential features of the data are present. This figure indicates that the vortex locations are

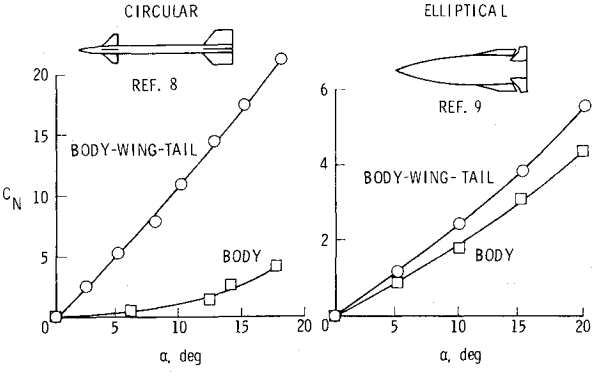

Fig. 5 Effect of body shape on experimental loads. $\phi=0$ deg, $M=2.50$.

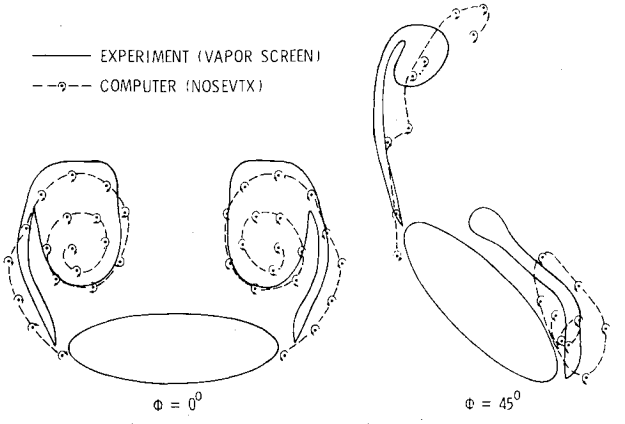

Fig. 6 Comparison of experimental and computed vortices on the sharp-nosed body. $X/L=1.0$, $\alpha=20$ deg, $M=2.50$.

being properly modeled by the vortex calculation procedure contained in the NOSEVTX code.

Pressure distribution comparisons for this body between the data presented earlier in this paper and NOSEVTX calculations are shown in Fig. 7. These results are for the 60% body station at angles of attack of 5, 10, and 20 deg. Since the roll angle is zero, comparisons are shown for only one side of the body. The NOSEVTX calculations are shown with and without the vortex model so that the linear-theory calculation and the vortex solution can be isolated. At 5 deg angle of attack, NOSEVTX predicts that no vortices will be shed, so that the NOSEVTX and linear solutions are identical. The agreement with data is excellent except in the outboard regions of the windward surface (45 deg $<\theta<$ 90 deg) where the theory slightly underpredicts the pressures. At 10 deg angle of attack, vortices are shed by NOSEVTX, but the vortex influence is primarily in the leading-edge region. The underprediction of the outboard windward pressures is very prominent at this angle of attack. The difference between the linear-theory pressure estimate and the experimental data, which increases with increasing angle of attack, represents a nonlinear attached-flow effect, as will be demonstrated subsequently. At the highest angle of attack, $\alpha=20$ deg, the calculated vortices are seen to have a substantial effect on the leeward pressure calculations. The NOSEVTX pressures show a definite improvement over the linear-theory calculations on the leeward surface of this body at this angle of attack. Note that the expansion pressure plateau is an artificially imposed vacuum limit in the NOSEVTX code.

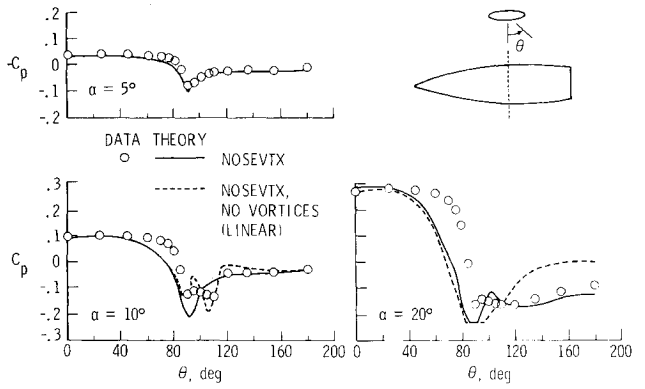

Fig. 7 Comparison of experimental and NOSEVTX pressure distributions on the sharp-nosed body. $X/L=0.60$, $\phi=0$ deg, $M=2.50$.

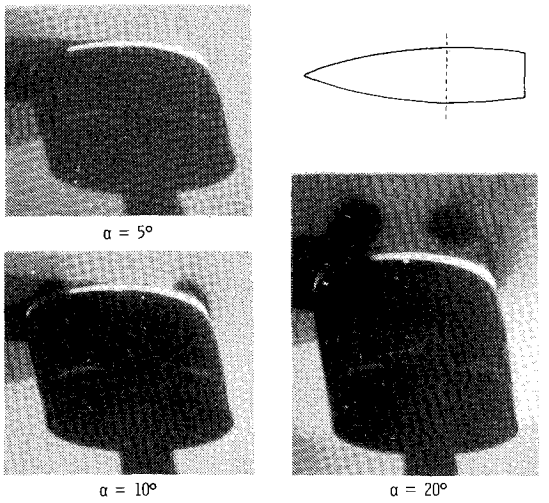

Fig. 8 Vapor-screen photographs of the sharp-nosed body. $X/L=0.64$, $\phi=0$ deg, $M=2.50$.

The extent of the predicted separation shown in this figure can also be experimentally verified by comparing the pressure results of Fig. 7 with vapor-screen photographs shown in Fig. 8. These vapor screens were taken on the same body at the same angles of attack and roll as the pressure results of Fig. 7. As discussed in Fig. 7, the NOSEVTX code predicts no vortices at $\alpha=5$ deg, weak vortices affecting primarily the regions near the sides of the body at $\alpha=10$ deg, and strong vortices affecting the entire leeward surface at $\alpha=20$ deg. The vapor screens of Fig. 8 confirm this result by showing no vortices at $\alpha=5$ deg, small vortices confined to the outboard regions of the body at $\alpha=10$ deg, and strong vortices covering most of the leeward side of the body at $\alpha=20$ deg.

Therefore, two types of nonlinear effects are seen by examining the pressure data in Fig. 7: 1) the separated-flow nonlinearities on the leeward surface, and 2) the attached-flow nonlinearities on the windward surface. The vortex model contained in the NOSEVTX code has been shown to calculate vortex influences which are in good agreement with experimental data. On the windward surface of the model, however, where the flow is attached, the linear theory underpredicts the pressure on the outboard regions even though the inboard calculations are in excellent agreement with the data.

NCOREL Code

Figure 9 is the repeat of Fig. 7 with the pressure calculations from the NCOREL code added. Comparing the experimental data with the nonlinear potential and the linear potential solutions clearly illustrates the nonlinear attached-flow effect which occurs for 0 deg $\leq\theta\leq$ 90 deg. This error in linear-theory pressure estimate for 0 deg $\leq\theta\leq$ 90 deg is due to the small-disturbance assumption inherent in the linear theory. These comparisons show that the pressures near the centerline region, both windward and leeward, are relatively unaffected by the small disturbance assumption even at high angles of attack. Also, the isentropic flow assumption of the potential method apparently does not affect the NCOREL pressure estimate adversely as long as the flow is attached. The error in the NCOREL calculations once the flow separates is seen in Fig. 9, especially for the $\alpha=20$ deg case. The NCOREL pressure estimates in the separated-flow region tend to "average out" on the leeside because of the large overexpansion on the outboard portion of the leeside (90 deg $\leq\theta\leq$ 130 deg) and the overcompression on the inboard portion of the leeside (130 deg $\leq\theta\leq$ 180 deg). Unfortunately, the regions of separated flow cannot be identified from NCOREL calculations alone without resorting to comparison with experimental data or more accurate solution techniques.

A correlation of flow separation with the departure of the NCOREL pressure estimate from the experimental data is shown in Fig. 10. In this figure, both vapor-screen photographs and experimental and NCOREL pressure

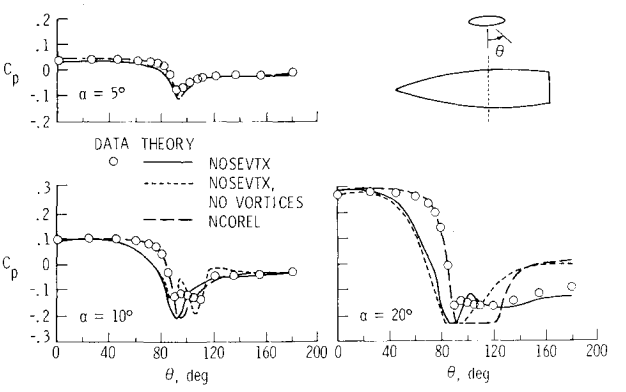

Fig. 9 Comparison of experimental and NCOREL pressure distributions on the sharp-nosed body. $X/L=0.60$, $\phi=0$ deg, $M=2.50$.

distributions are shown for the sharp-nosed body alone at an angle of attack of 10 deg and zero roll angle. Data for two body stations are shown—the 30 and 95% stations. At the forward station, the vapor-screen photograph shows no vortices. Since separation has not occurred at this station, the NCOREL pressure prediction is accurate on both the windward and leeward surfaces. At the rearward station, however, the vapor screen shows that vortices are present. The corresponding pressure plot shows that NCOREL does not calculate pressures accurately in the separated flow, since this phenomenon is not modeled by the governing equation. However, the point at which the NCOREL pressure estimate departs from the experimental data closely corresponds to the beginning of the separation region as defined by the vapor-screen photograph.

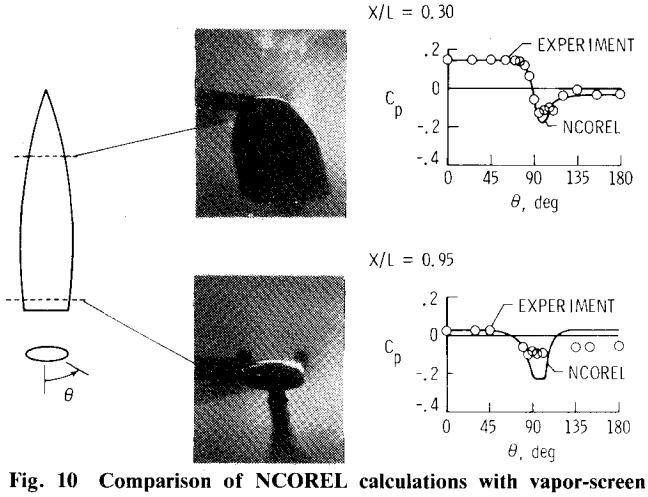

Fig. 10 Comparison of NCOREL calculations with vapor-screen data on the sharp-nosed body. $\alpha = 10$ deg, $\phi = 0$, $M = 2.50$.

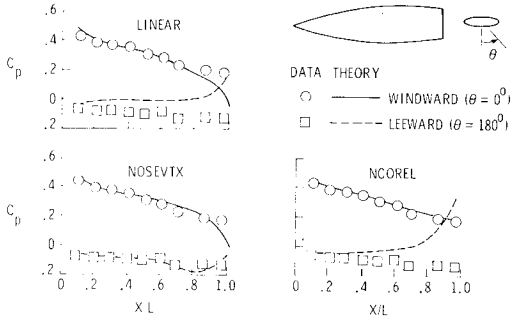

Fig. 11 Centerline pressure distributions on the sharp-nosed body. $\alpha = 20$, $\phi = 0$, $M = 2.50$.

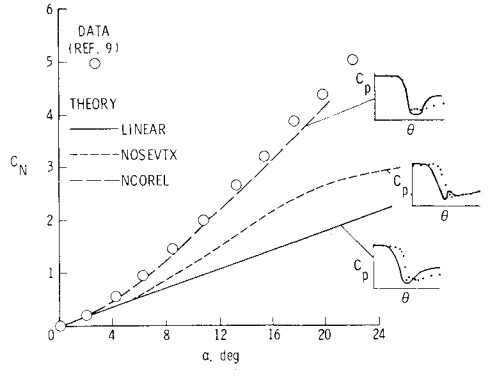

Fig. 12 Comparison of experimental and computed loads on the sharp-nosed body. $\phi = 0$ deg, $M = 2.50$.

Centerline Pressure Comparisons

Figure 11 shows a summary of the code comparisons with data for the windward and leeward centerlines along the entire length of the body. These data are for 20 deg angle of attack and zero roll angle on the sharp-nosed body alone.

Observation of the centerline pressures shows that the linear theory predicts the windward pressures quite well except near the aft end of the body, even though it has been shown previously that significant errors occur in the windward pressures in the vicinity of the leading edge. This observation points out the importance of looking at the spanwise pressure distribution on bodies such as this and not just the centerline predictions.

The NOSEVTX centerline predictions show very good agreement with the data. Comparing the leeward centerline predictions with those of the linear-theory solution demonstrates how well the vortex model in NOSEVTX works over the entire length of the model. These NOSEVTX centerline predictions again emphasize the importance of not relying on centerline predictions alone to evaluate overall code performance on bodies such as these.

The NCOREL centerline predictions are similar to the linear-theory predictions although the circumferential pressure plots shown earlier show that the NCOREL code is superior to linear theory.

Normal-Force Comparisons

Figure 12 shows the prediction from these computational methods for the overall normal force on the sharp-nosed body alone over the entire angle-of-attack range at zero roll angle. The normal-force predictions are simply an integration of the calculated pressure distributions, and the experimental data are from internal strain-gage balance measurements taken from Ref. 9. The small pressure distribution inserts used to explain trends in the data are taken from the figure shown previously at the 60% body station and 20 deg angle of attack.

It can be seen that linear theory badly underestimates the normal force. This is consistent with the pressure data which show that the pressures are underpredicted on the outboard part of the windward surface and overpredicted on the leeward surface. For the thin wing applications, linear theory often gives good overall load estimates even though it badly predicts the pressures. In these instances, the good load estimates are due to compensating errors in the predictions for windward and leeward surfaces. Note that this compensating effect is not present in these body data, resulting in badly underpredicted loads.

The NOSEVTX estimation shows a definite improvement over linear theory, but the underprediction of the outboard windward pressures results in a loads prediction that is still far below the data. The difference between the linear-theory and NOSEVTX curves represents the nonlinear leeside vortex effects, whereas the difference between the NOSEVTX curve and the experimental data represents the nonlinear attached-flow effects on the windward surface.

The NCOREL predictions show very good agreement with the data, although the separated-flow effects are not treated in this method. The accurate normal force estimates from NCOREL are due to the accurate attached-flow estimates and a compensating error which occurs in the separated-flow region as was mentioned in the discussion for Fig. 9.

Conclusions

A study has been made to determine the capability of state-of-the-art and advanced computational methods for analysis of missile body shapes with elliptical cross sections. Comparisons have been made with surface-pressure and normal force data to investigate the capability of two computational methods—NOSEVTX and NCOREL—to predict the aerodynamics of such bodies. Based on the results of these comparisons, the following conclusions have been drawn.

1) Two types of nonlinear flow were observed: separated-flow nonlinearities on the leeward surface, and attached-flow nonlinearities on the windward surface.

2) Neither code adequately calculated both types of nonlinearities; however, the NCOREL code provided extremely accurate pressure estimates for attached-flow conditions, whereas the NOSEVTX code accurately calculated body vortices and leeside pressures.

Acknowledgment

The authors gratefully acknowledge assistance of Dr. Michael J. Siclari of the Grumman Aerospace Corporation with the NCOREL code.

References

[1]Graves, E. B. and Robins, A. W., "Supersonic Aerodynamic Trade Data for a Low-Profile Monoplanar Missile Concept," *Journal of Aircraft*, Vol. 17, Feb. 1980, pp. 95-98.

[2]Graves, E. B., "Aerodynamic Characteristics of a Monoplanar Missile Concept with Bodies of Circular and Elliptical Cross Sections," NASA TM-74079, Dec. 1977.

[3]Dillenius, M. F. E. and Nielsen, J. N., "Computer Programs for Calculating Pressure Distributions Including Vortex Effects on Supersonic Monoplane or Cruciform Wing-Body-Tail Combinations with Round or Elliptical Bodies," NASA CR-3122, April 1979.

[4]Mendenhall, M. R., "Prediction of Vortex Shedding from Circular and Noncircular Bodies in Supersonic Flow," Nielsen Engineering and Research, Inc., Mountain View, Calif., TR-239, Nov. 4, 1981.

[5]Mendenhall, M. R. and Allen, J. M., "Prediction of Vortex Shedding from Noncircular Bodies at High Angles of Attack in Supersonic Flow," 51st Meeting of the Fluid Dynamics Panel. AGARD Symposium on Missile Aerodynamics, Trondheim, Norway, Sept. 1982.

[6]Allen, J. M., "Comparison of Analytical and Experimental Supersonic Aerodynamic Characteristics of a Forward Control Missile," AIAA Paper 81-0398, Jan. 1981.

[7]Allen, J. M. and Blair, A. B., Jr., "Comparison of Analytical and Experimental Supersonic Aerodynamic Characteristics of a Forward Control Missile," *Journal of Spacecraft and Rockets*, Vol. 19, March-April 1982, pp. 155-159.

[8]Blair, A. B. Jr., Allen, J. M., and Hernandez, G., "Effect of Tail-Fin Span on Stability and Control Characteristics of a Forward Control Missile at Supersonic Speeds," NASA TP-2157, 1983.

[9]Graves, E. B. and Fournier, R. H., "Effect of Nose Bluntness and Afterbody Shape on Aerodynamic Characteristics of a Monoplanar Missile Concept with Bodies of Circular and Elliptical Cross Sections at a Mach Number of 2.50," NASA TM-80055, 1979.

[10]Allen, J. M., Hernandez, G., and Lamb, M., "Body Surface Pressure Data on Two Monoplane-Wing Missile Configurations with Elliptical Cross Sections at Mach 2.50," NASA TM-85645, Sept. 1983.

[11]Siclari, M. J., "The NCOREL Computer Program for 3D Nonlinear Supersonic Potential Flow Computations," NASA CR-3694, 1983.

[12]Adams, M. C., "Determination of Shapes of Boattail Bodies of Revolution for Minimum Wave Drag," NACA TN-3054, 1953.

[13]Jackson, C. M., Jr., Corlett, W. A., and Monta, W. J., "Description and Calibration of the Langley Unitary Plan Wind Tunnel," NASA TP-1905, Nov. 1981.

[14]Dillenius, M. F. E., "Program LRCDM2, Improved Aerodynamic Prediction Program for Supersonic Canard-Tail Missiles with Axisymmetric Bodies," Nielsen Engineering and Research, Inc., Mountain View, Calif., TR-287, March 1983.

[15]Siclari, M. J., "Computation of Nonlinear Supersonic Potential Flow over Three-Dimensional Surfaces," *Journal of Aircraft*, Vol. 20, May 1983, pp. 462-468.

[16]Laiosa, J. P. and Boppe, C. W., "A New Hybrid Approach to Supersonic Aircraft Analysis," AIAA Paper 83-0340, Jan. 1983.